J Mater Sci: Mater Electron (2017) 28:10564–10572
DOI 10.1007/s10854-017-6830-9

Multicolor emission in lithium-aluminum-zinc phosphate glasses activated with Dy^{3+}, Eu^{3+} and Dy^{3+}/Eu^{3+}

A. N. Meza-Rocha[1] · A. Speghini[2,3] · J. Franchini[2] · R. Lozada-Morales[4] · U. Caldiño[5]

Received: 17 January 2017 / Accepted: 23 March 2017 / Published online: 3 April 2017

Abstract A spectroscopic analysis of Dy^{3+}, Eu^{3+} and Dy^{3+}/Eu^{3+} doped lithium-aluminum-zinc phosphate glasses is carried out based on absorption and photoluminescence spectra and decay time measurements. According to the CIE1931 chromaticity coordinates and correlated color temperature (*CCT*), neutral white and reddish-orange global emissions were observed in the Dy^{3+} and Eu^{3+} singly-doped glasses, respectively, after excitations of Dy^{3+} at 348 nm and Eu^{3+} at 393 nm. A high red color purity of 97.2% is achieved in the Eu^{3+} singly-doped glass excited at 393 nm. Upon Dy^{3+} excitation at 348 nm, the Dy^{3+}/Eu^{3+} doped glass showed warm white overall emission, with *CCT* value of 3629 K. Upon Dy^{3+} and Eu^{3+} co-excitations at 362, 381 and 387 nm, the Dy^{3+}/Eu^{3+} doped glass showed reddish-orange overall emissions, with *CCT* values in the 1620–2385 K range, depending on the excitation wavelength. In the Dy^{3+}/Eu^{3+} doped glass excited at 348 nm, the warm white emission was achieved by a non-radiative energy transfer from Dy^{3+} to Eu^{3+} with an efficiency and probability of 0.08 and 89.51 s^{-1}, respectively. The dominant mechanism could be through an electric quadrupole–quadrupole interaction, as it is suggested from the Inokuti-Hirayama model. A back non-radiative energy transfer from Eu^{3+} to Dy^{3+} is also observed, which could also be mediated by an electric quadrupole–quadrupole interaction. The Eu^{3+} to Dy^{3+} energy transfer efficiency and probability being of 0.08 and 30.00 s^{-1}, respectively.

1 Introduction

Due to its $^4F_{9/2} \rightarrow {}^6H_{13/2}$ (~480 nm), $^4F_{9/2} \rightarrow {}^6H_{15/2}$ (~573 nm), $^6H_{11/2} \rightarrow {}^6H_{13/2}$ (~1.34 μm) and $^6H_{13/2} \rightarrow {}^6H_{15/2}$ (~3.02 μm) emission bands, the incorporation of Dy^{3+} into a great variety of hosts has received considerable attention for W-LED, solid state laser and optical amplifier applications, among others [1–3]. By adjusting the relative blue ($^4F_{9/2} \rightarrow {}^6H_{13/2}$) and yellow ($^4F_{9/2} \rightarrow {}^6H_{15/2}$) emission intensities, it is possible to generate white light emission in Dy^{3+} singly-activated phosphors upon near-ultraviolet (NUV) excitation [4, 5], making Dy^{3+} a very attractive ion for W-LED applications. However, the negligible red emission of Dy^{3+} singly-doped phosphors represents a drawback to modulate and produce warm white light. In order to overcome this deficiency, Eu^{3+} ions are introduced to contribute with a red component, generating by this way tunable white emission [4–6]. Such emission can be achieved by an efficient $Dy^{3+} \rightarrow Eu^{3+}$ energy transfer process upon NUV excitation, which matches well with the emission for instance of InGaN-based LED. Among the hosts tested for the incorporation of Dy^{3+}, Eu^{3+} and Dy^{3+}/Eu^{3+}, phosphate

✉ A. N. Meza-Rocha
anehemiasme@conacyt.mx

1 CONACYT- Benemérita Universidad Autónoma de Puebla, Postgrado en Física Aplicada, Facultad de Ciencias Físico-Matemáticas, Av. 14 Sur Y Av. San Claudio, Col. San Manuel, Puebla, Mexico

2 Dipartimento di Biotecnologie, Università di Verona, and INSTM, Udr Verona, Strada Le Grazie 15 37314 Verona, Italy

3 IFAC CNR, Nello Carrara Institute of Applied Physics, 50019 Sesto Fiorentino, Italy

4 Benemérita Universidad Autónoma de Puebla, Postgrado en Física Aplicada, Facultad de Ciencias Físico-Matemáticas, Av. 14 sur y Av. San Claudio, Col. San Manuel, Puebla, Mexico

5 Departamento de Física, Universidad Autónoma Metropolitana-Iztapalapa, P.O. Box 55-534, 09340 México D.F., Mexico

glasses possess unique characteristics, such as low melting temperature, high transparency in the NUV–Vis range, high thermal expansion, high luminous ion concentration, large emission and absorption cross section, among others [7–9]. However, their poor chemical durability is an inconvenience for many applications [8, 10]. As a solution, it has been reported that ZnO improves the chemical stability because Zn^{2+} is able to form ZnO_4 tetrahedron and/or P–O–Zn bridges through phosphate chain linkages in the glassy structure [9]. Furthermore, the combination of lithium and aluminum in phosphate glasses offers high transparency and thermal stability. All these characteristics make lithium–aluminum–zinc phosphate glass very attractive for potential W-LED applications [9, 11]. Thus, in this work a spectroscopy study based on absorption, excitation and emission spectra, and decay time profiles of lithium–aluminum zinc phosphate glasses activated with Eu^{3+}, Dy^{3+} and Dy^{3+}/Eu^{3+} is presented.

2 Experimental details

The molar compositions of the lithium–aluminum–zinc phosphate glasses under investigation were 5.0 Li_2O–5.0 Al_2O_3–39.5 ZnO–50.0 P_2O_5–0.5 Dy_2O_3, 5.0 Li_2O–5.0 Al_2O_3–39.0 ZnO–50.0 P_2O_5–1.0 Eu_2O_3, 5.0 Li_2O–5.0 Al_2O_3–38.5 ZnO–50.0 P_2O_5–0.5 Dy_2O_3–1.0 Eu_2O_3, which will be referred hereafter as LAZD, LAZE and LAZDE, respectively. The glasses were synthetized by mixing stoichiometric amounts of reagent grade $NH_4H_2PO_4$, ZnO, Li_2CO_3, Al_2O_3, Dy_2O_3 and Eu_2O_3 in a sintered alumina crucible and melting the mixture for 6 h at 1250 °C. The melts then were quenched onto a copper plate. The glasses were annealed at 350 °C for 16 h to obtain thermal and mechanical stability. Photoluminescence spectra were recorded by a Horiba Jobin–Yvon Fluorolog 3–22 spectrofluorometer operating with a 450 W ozone-free Xe lamp in the steady mode or with a pulsed Xe lamp for decay time profile measurements. The decay times were recorded in the phosphorescence mode using a delay time of 0.01 ms after the excitation pulse (3 µs half-width) and a 5 ms sample window. The absorption spectra were recorded by a Carry 5000 spectrometer. All measurements were carried out at room temperature.

3 Results and discussion

3.1 LAZD glass phosphor

Figure 1a shows the characteristic absorption spectrum of the LAZD glass on the 300–770 nm range. It consists of several bands centered at about 324, 348, 364, 386, 425, 452, 474 and 750 nm, corresponding to Dy^{3+} ion $^4K_{15/2}$, ($^4M_{15/2}$,$^6P_{7/2}$), $^4I_{11/2}$, ($^4K_{17/2}$,$^4M_{19/2,21/2}$,$^4I_{13/2}$,$^4F_{7/2}$), $^4G_{11/2}$, $^4I_{15/2}$, $^4F_{9/2}$ and $^6F_{1/2}$ + $^6F_{3/2}$, respectively. The absorption spectrum on the 800–1800 nm range displayed in Fig. 1b, shows bands at 886, 1094, 1266 and 1677 nm, associated with the Dy^{3+} ions $^6H_{5/2}$ + $^6F_{7/2}$, $^6H_{7/2}$ + $^6F_{9/2}$, $^6H_{9/2}$ + $^6F_{11/2}$ and $^6H_{11/2}$ transitions from the $^6H_{15/2}$ ground state, respectively. The absorption edge located below 340 nm reveals a high host transparency, which fulfills the requirements for optical applications in the visible range.

The emission spectrum, exciting into the $^6H_{15/2}$ → ($^4M_{15/2}$,$^6P_{7/2}$) absorption transition at 348 nm (Fig. 1c), displays the typical Dy^{3+} emissions centered at 454, 483, 572 and 661 nm, associated with the $^4I_{15/2}$ → $^6H_{15/2}$, $^4F_{9/2}$ → $^6H_{15/2}$, $^6H_{13/2}$ and $^6H_{11/2}$ Dy^{3+} ion transitions, respectively. These emissions are originated by an initial population from the ($^4M_{15/2}$,$^6P_{7/2}$) state, which non-radiatively relaxes to the $^4F_{9/2}$ emitting level, giving rise to the blue, yellow and red Dy^{3+} emissions. The feeble $^4I_{15/2}$ → $^6H_{15/2}$ emission at 454 nm is related with a non-radiative relaxation from the $^4I_{15/2}$ state to the $^4F_{9/2}$ one, as consequence of the small energy gap (~1000 cm^{-1}) between the $^4I_{15/2}$ and $^4F_{9/2}$ levels (see Fig. 2). On the other hand, the intensity ratio of the $^4F_{9/2}$ → $^6H_{13/2}$ (yellow) and $^4F_{9/2}$ → $^6H_{15/2}$ (blue) transitions dominates the emission tonality, and it is associated with the predominant symmetry around Dy^{3+} ions into the host. It is well known that emissions with $\Delta J = 0, \pm1, \pm3$ correspond to magnetic dipole (MD) transitions, and they are insensitive to the host environment, whereas emissions, with $\Delta J = \pm 2, \pm4, \pm6$, are associated with hypersensitive transitions to the host environment. So that, when Dy^{3+} is mainly located into a non-inversion symmetry site, the intensity of the $^4F_{9/2}$ → $^6H_{13/2}$ emission is significantly higher than that of the $^4F_{9/2}$ → $^6H_{15/2}$ emission. Thus, the ($^4F_{9/2}$ → $^6H_{13/2}$)/($^4F_{9/2}$ → $^6H_{15/2}$) emission intensity ratio can be used to evaluate the predominant symmetry around Dy^{3+} into the lithium–aluminum zinc phosphate glass host. In this case, the ($^4F_{9/2}$ → $^6H_{13/2}$)/($^4F_{9/2}$ → $^6H_{15/2}$) emission intensity ratio resulted to be 1.57, suggesting that Dy^{3+} ions are mostly distributed into non-inversion symmetry sites. Thereby, neutral white emission is obtained from the LAZD glass according to its $x = 0.367$ and $y = 0.412$ CIE1931 chromaticity coordinates and correlated color temperature (*CCT*) of 4547 K, as calculated by the following Eq. [12]:

$$CCT = 449n^3 + 3525n^2 + 6823.8n + 5520.33, \quad (1)$$

where $n = (x - 0.3320)/(0.1858 - y)$, and x and y are the chromaticity coordinates.

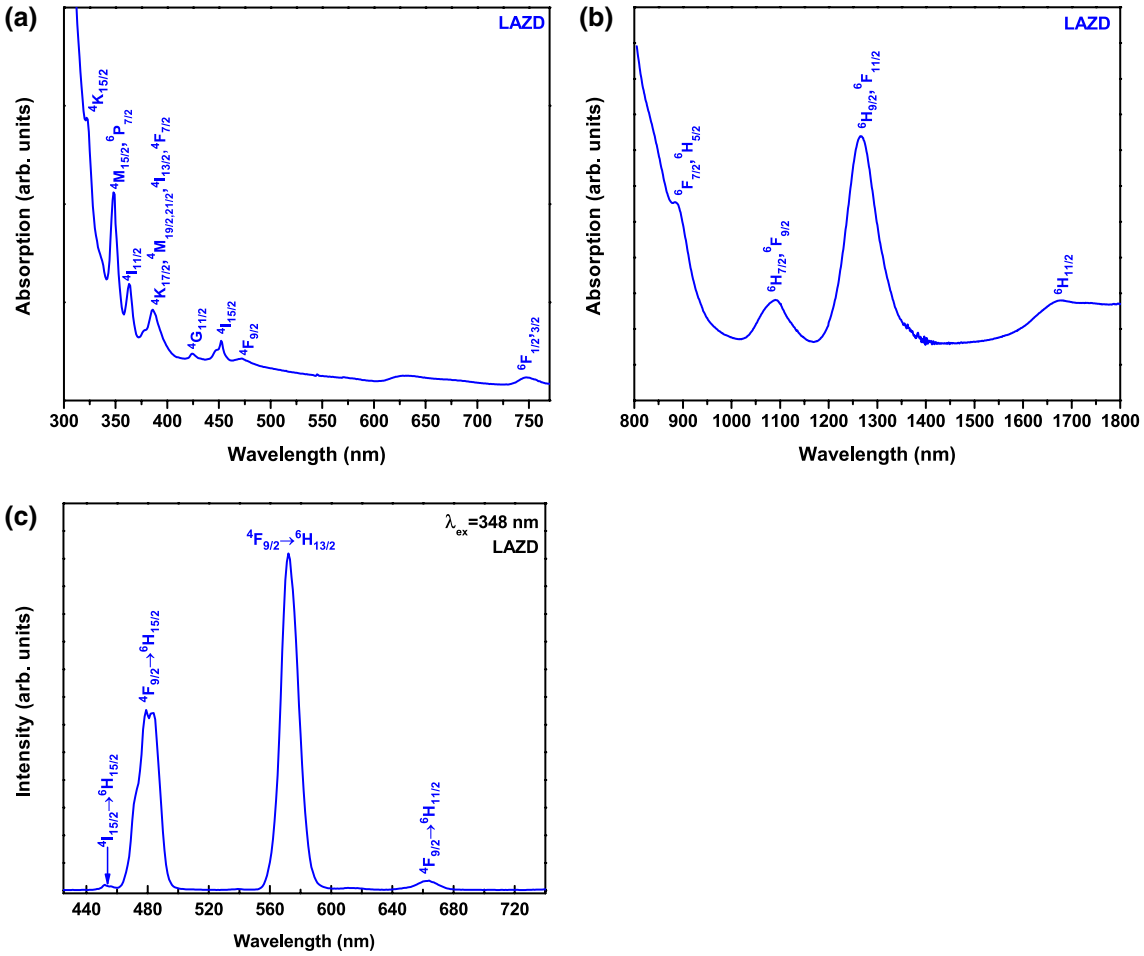

Fig. 1 Absorption on the **a** 300–770 and **b** 800–1600 nm ranges and **c** emission spectra of the LAZD glass

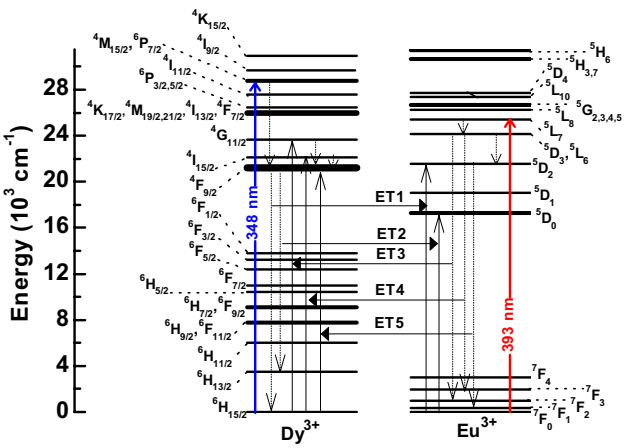

Fig. 2 Dy^{3+} and Eu^{3+} energy level diagram illustrating the possible energy transfer pathways among the Dy^{3+} and Eu^{3+} ions

3.2 LAZE glass phosphor

The absorption spectrum of the LAZE glass (Fig. 3a) shows eight bands located at 318, 362, 375, 382, 393, 415, 465 and 533 nm, corresponding to transitions of the $^5H_6$, $^5D_4$, $^5G_{2,3,4,5}$, $^5L_8$, $^5L_7$, $^5D_3$, $^5D_2$ and $^5D_1$ Eu^{3+} excited states, respectively. The emission spectrum, upon 393 nm excitation into the $^5L_7$ predominant absorption, exhibits the Eu^{3+} emissions centered at 577, 591, 611, 651 and 699 nm, associated with the $^5D_0 \rightarrow {}^7F_0$, $^5D_0 \rightarrow {}^7F_1$, $^5D_0 \rightarrow {}^7F_2$, $^5D_0 \rightarrow {}^7F_3$ and $^5D_0 \rightarrow {}^7F_4$ electronic transitions, respectively (Fig. 3b). Such emissions are achieved after non-radiative relaxations from the $^5L_7$ state to the $^5D_0$ one, through the ($^5D_3$,$^5L_6$), $^5D_2$ and $^5D_1$ intermediate levels (see Fig. 2). Similarly to the dysprosium emissions, the europium $^5D_0 \rightarrow {}^7F_2/{}^5D_0 \rightarrow {}^7F_1$ emission intensity ratio is useful to test the dominant symmetry around Eu^{3+} [4]. If Eu^{3+} ions occupy non-inversion symmetry sites,

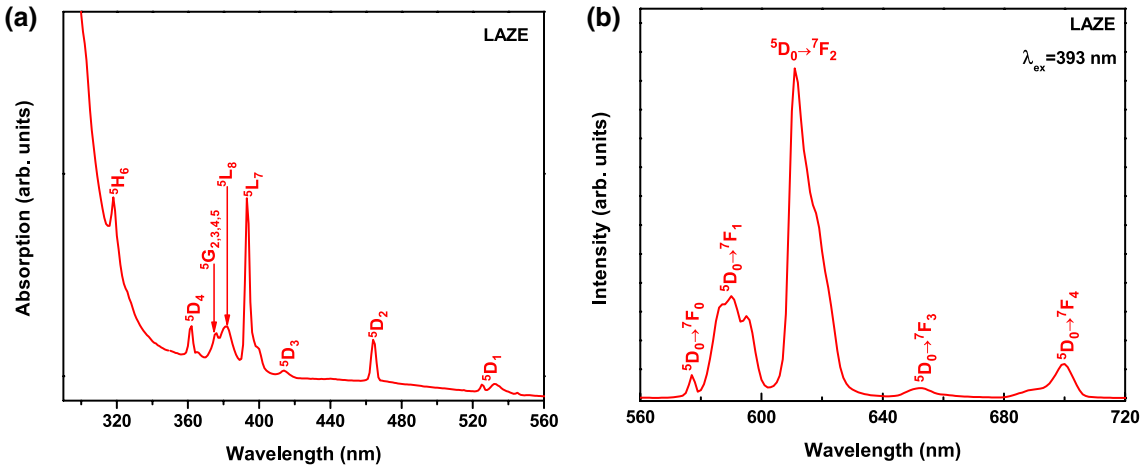

Fig. 3 **a** Absorption and **b** emission spectra of the LAZE glass

the intensity of the $^5D_0 \rightarrow {}^7F_2$ emission should be higher than that of the $^5D_0 \rightarrow {}^7F_1$ emission. In this case, the $^5D_0 \rightarrow {}^7F_2/{}^5D_0 \rightarrow {}^7F_1$ emission intensity ratio is around 2.56, suggesting that like Dy^{3+} ions, Eu^{3+} ions mainly occupy sites without inversion symmetry. The overall emission of the LAZE glass upon 393 nm excitation was also characterized by the CIE1931 chromaticity coordinates and correlated color temperature (*CCT*), resulting in values of $x = 0.638$ and $y = 0.354$, and 2070 K, respectively. Such color coordinates are within the reddish-orange region, with a high red color purity of 97.2%. The color purity was estimated from the the weighted average of the sample emission colour coordinates (x_s, y_s) relative to the CIE1931 Standard Source C illuminant coordinates (x_i, y_i) and the dominant wavelength coordinates (x_d, y_d) relative to the (x_i, y_i) coordinates, through the following relation [13]:

$$\text{Color purity} = \frac{\sqrt{(x_s - x_i)^2 + (y_s - y_i)^2}}{(x_d - x_i)^2 + (y_d - y_i)^2} \times 100\% \quad (2)$$

where the coordinates (x_d, y_d) are those of the monochromatic wavelength having the same color as the light source. The dominant wavelength is determined by drawing a straight line from the (x_i, y_i) coordinates through the (x_s, y_s) coordinates until the line intersects to the outer locus of points along the spectral edge of the CIE1931 chromaticity diagram.

3.3 LAZDE glass phosphor

In order to study the effect of Dy^{3+} co-doping on the Eu^{3+} excitation, Fig. 4a displays the excitation spectra of the LAZDE and LAZE glasses monitoring the europium $^5D_0 \rightarrow {}^7F_2$ emission at 611 nm, wherein Dy^{3+} does not emit

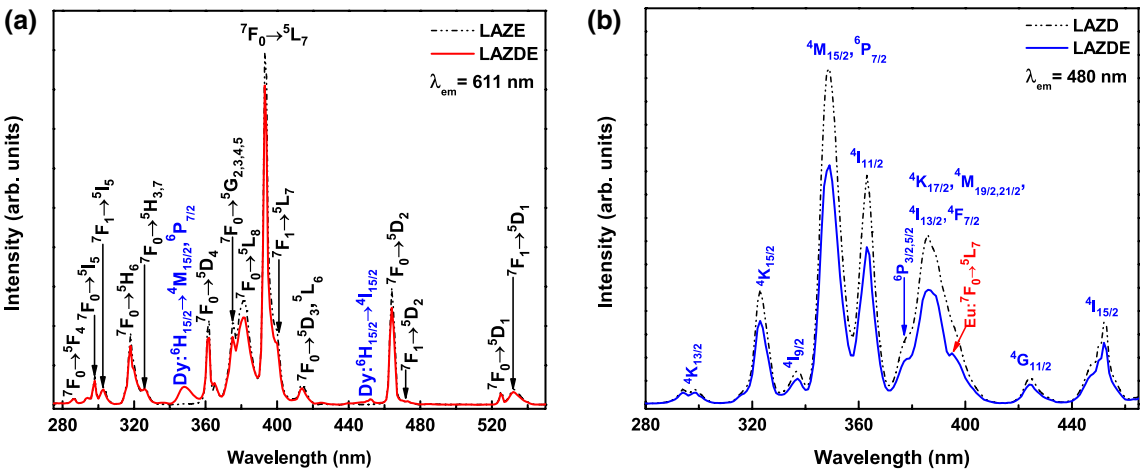

Fig. 4 Excitation spectra of the glasses **a** LAZE and LAZDE and **b** LAZD and LAZDE monitoring the Eu^{3+} and Dy^{3+} emissions at 611 and 480 nm, respectively

(see Fig. 1c). Besides the Eu^{3+} characteristic excitation bands, the excitation spectrum of the LAZDE glass shows two additional bands centered at 348 and 452 nm, related with the dysprosium $^6H_{15/2} \rightarrow (^4M_{15/2},^6P_{7/2})$ and $^4I_{15/2}$ excitations, respectively, suggesting that Dy^{3+} sensitizes Eu^{3+}. This process leads to Eu^{3+} emission through the Dy^{3+} excitation. The europium excitation band intensity in the LAZDE glass is lower than in the LAZE one, which could be evidencing $Eu^{3+} \rightarrow Dy^{3+}$ energy transfer, as discussed below.

Figure 4b depicts the excitation spectra of the LAZDE and LAZD glasses recording the dysprosium $^4F_{9/2} \rightarrow {}^6H_{15/2}$ emission at 480 nm, wherein Eu^{3+} is not able to emit. The excitation spectrum of the LAZDE glass displays, in addition to the Dy^{3+} transitions, a shoulder mounted on the dysprosium $^6H_{15/2} \rightarrow (^4K_{17/2},^4M_{19/2,21/2},^4I_{13/2},^4F_{7/2})$ excitation band, which matches with the europium $^7F_0 \rightarrow {}^5L_7$ excitation, pointing out a feasible $Eu^{3+} \rightarrow Dy^{3+}$ energy transfer process. Also, it can be noticed that the dysprosium excitation band intensity in the co-doped glass (LAZDE) is lower than in the singly doped one (LAZD). This fact might be associated with $Dy^{3+} \rightarrow Eu^{3+}$ energy transfer according to the Dy^{3+} excitation bands observed by monitoring the isolated Eu^{3+} emission.

In order to clarify the mechanism involved in the $Dy^{3+} \rightarrow Eu^{3+}$ energy process, Fig. 5a shows the decay profiles of the isolated dysprosium $^4F_{9/2} \rightarrow {}^4H_{15/2}$ emission at 480 nm under excitation at 348 nm of the LAZD and LAZDE glasses. The emission of the Dy^{3+} singly doped glass (LAZD) follows a non-exponential decay, attributed to cross relaxation processes among Dy^{3+} ions [14]. In presence of Eu^{3+}, the decay remains non-exponential and becomes shorter, suggesting a non-radiative $Dy^{3+} \rightarrow Eu^{3+}$ energy transfer process. Because both decays are not exponential the lifetime was taken as the average lifetime [15], resulting to be 0.92 and 0.85 ms for the LAZD and LAZDE glasses, respectively. So that, the $Dy^{3+} \rightarrow Eu^{3+}$ energy transfer process is accomplished with an efficiency and probability of 0.08 and 89.51 s^{-1}, respectively [16]. According to the Dy^{3+} and Eu^{3+} energy levels and overlap region of the Dy^{3+} emission and Eu^{3+} absorption portrayed in Fig. 5b, this process could be achieved through the following channels illustrated in Fig. 2 [15, 17]:

ET1: $^4F_{9/2}(Dy^{3+}) + {}^7F_{0,1}(Eu^{3+}) \rightarrow {}^6H_{15/2}(Dy^{3+}) + {}^5D_2(Eu^{3+})$ and.

ET2: $^4F_{9/2}(Dy^{3+}) + {}^7F_{0,1}(Eu^{3+}) \rightarrow {}^6H_{13/2}(Dy^{3+}) + {}^5D_0(Eu^{3+})$.

The dominant electrostatic mechanism involved in the $Dy^{3+} \rightarrow Eu^{3+}$ energy transfer process is inferred by fitting the emission decay at 480 nm of the Dy^{3+} and Eu^{3+} co-doped glass with the Inokuti-Hirayama model given as follows [18]:

$$I(t) = I_o \exp\left(-\frac{t}{\tau_0} - \gamma_s t^{3/S}\right) \quad (3)$$

where I_0 is the intensity at $t=0$, $\tau_0$is the donor (Dy^{3+}) lifetime in absence of acceptors (Eu^{3+}), γ_s is a measure of the direct energy transfer and S is the multipolar interaction parameter. The latter one can take values of 6, 8 and 10 for electric dipole–dipole (d–d), dipole–quadrupole (d–q) and quadrupole–quadrupole (q–q) interactions, respectively. The best fitting was achieved for $S=10$, with $\gamma_{10} = 5.24\ s^{-3/10}$ (see Fig. 5a). Therefore, it is inferred that an electric quadrupole–quadrupole interaction might dominate the $Dy^{3+} \rightarrow Eu^{3+}$ energy transfer process, as expected from the inter-4f transitions of the interacting ions.

The R_c critical energy transfer distance and $\gamma_S$parameter are related as follows:

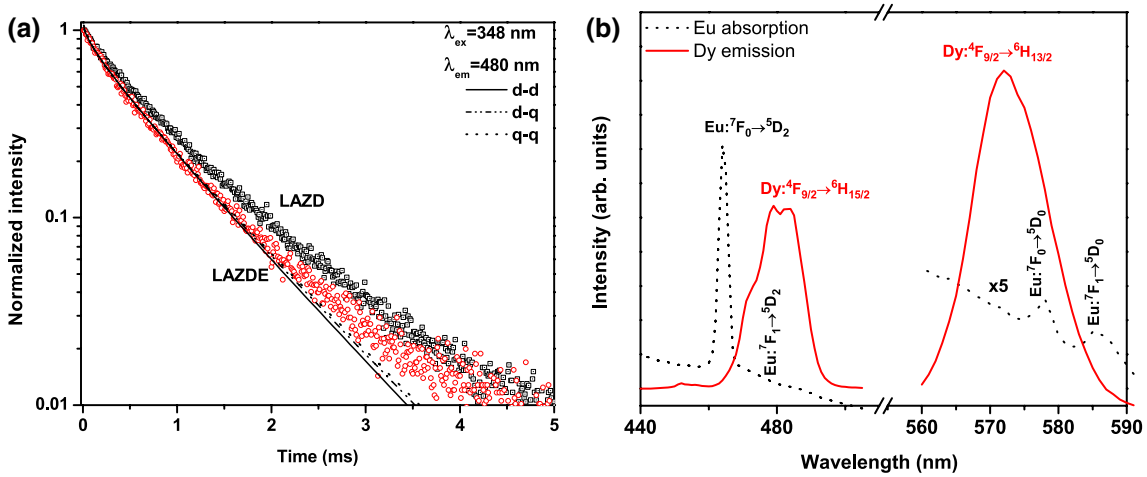

Fig. 5 Decay time profiles of **a** Dy^{3+} emission at 480 nm for the LAZD and LAZDE glasses. *Solid lines* represent the best fitting by using Eq. (3), and **b** overlap region of the Dy^{3+} emission and Eu^{3+} absorption

$$\gamma_S = \frac{4\pi}{3}\Gamma\left(1-\frac{3}{S}\right)\rho_a\left(\frac{R_c}{\frac{1}{\tau_0}/S}\right)^3 \quad (4)$$

In this equation, $\rho_a$is the acceptor (in this case Eu^{3+}) concentration (8.9×10^{19} ions cm^{-3}), τ_0 is the donor average lifetime in absence of acceptors and $\Gamma(1-\frac{3}{S})$ is the Euler´s gamma function, which takes values of 1.77, 1.43 and 1.30 for $S=6$, 8 and 10, respectively. Based on this relationship, the R_c critical distance for an electric quadrupole–quadrupole interaction resulted to be 11 Å. The Dy^{3+}–Eu^{3+} interaction distance for a random ion distribution [19], considering $\rho_{Dy}+\rho_{Eu} \approx 1.3\times10^{20}$ ions cm^{-3}, is around 24 Å. This distance is larger than the critical distance, suggesting that the $Dy^{3+} \rightarrow Eu^{3+}$ energy transfer predominantly arises from Dy–Eu clusters instead of from the randomly distributed ions.

With regard to the $Eu^{3+} \rightarrow Dy^{3+}$ energy transfer, Fig. 6a depicts the isolated Eu^{3+} emission decay profiles at 611 nm, under excitation at 393 nm, for the LAZE and LAZDE glasses. Unlike to the Dy^{3+} emission decay, in the singly Eu^{3+} doped glass (LAZE) the Eu^{3+} emission decay exhibits an almost exponential evolution. In the co-doped glass (LAZDE) the Eu^{3+} emission decay displays a non-exponential behavior at times shorter than 1 ms and it becomes faster, which reveals $Eu^{3+} \rightarrow Dy^{3+}$ non-radiative energy transfer. The average lifetimes of the Eu^{3+} emission resulted to be 2.82 and 2.60 ms for the LAZE and LAZDE glasses, respectively. These values suggest that the $Eu^{3+} \rightarrow Dy^{3+}$ energy transfer process is achieved with efficiency and probability of 0.08 and 30.00 s^{-1}, respectively [16]. Based on the Dy^{3+} and Eu^{3+} energy level diagram and overlap region of the Eu^{3+} emission and Dy^{3+} absorption showed in Fig. 6b, such process might arise through the following pathways (see Fig. 2) [15, 17]:

ET3: $^5D_3(Eu^{3+}) + {}^6H_{15/2}(Dy^{3+}) \rightarrow {}^7F_2(Eu^{3+}) + {}^4G_{11/2}(Dy^{3+})$,

ET4: $^5D_3(Eu^{3+}) + {}^6H_{15/2}(Dy^{3+}) \rightarrow {}^7F_3(Eu^{3+}) + {}^4I_{15/2}(Dy^{3+})$ and

ET5: $^5D_2(Eu^{3+}) + {}^6H_{15/2}(Dy^{3+}) \rightarrow {}^7F_1(Eu^{3+}) + {}^4F_{9/2}(Dy^{3+})$.

To infer the dominant electrostatic mechanism involved in the $Eu^{3+} \rightarrow Dy^{3+}$ energy transfer, the Eu^{3+} emission decay at 611 nm was fitted by Eq. (3). The best fitting was attained for $S=10$ with $\gamma_{10} = 2.12$ $s^{-3/10}$ (Fig. 6a), suggesting that the energy transfer from Eu^{3+} to Dy^{3+} might be mediated by a quadrupole–quadrupole electric interaction, in a similar way as the $Dy^{3+} \rightarrow Eu^{3+}$ energy transfer. In this case, the R_c distance determined by Eq. (4), for a Dy^{3+} acceptor concentration of 4.4×10^{19} ions cm^{-3}, is 12 Å, which is smaller than the Eu–Dy interaction distance assuming a random ion distribution (24 Å). Therefore, the $Eu^{3+} \rightarrow Dy^{3+}$ energy transfer might take place among Eu–Dy clusters.

3.4 CIE1931 chromaticity coordinates and correlated color temperature for different excitation wavelengths

By comparing the Dy^{3+} and Eu^{3+} relative excitation intensities illustrated in Fig. 4a, b, it can be observed that excitation wavelengths at 348, 362, 381 and 387 could be useful to modulate the relative intensity of the Dy^{3+} and Eu^{3+} emissions in order to produce different light tonalities. Such excitations are within emissions of commercial AlGaN (348 nm), GaN (360 nm) and InGaN (380–405 nm) LEDs [20–22]. Figures 7 and 8 show respectively, the

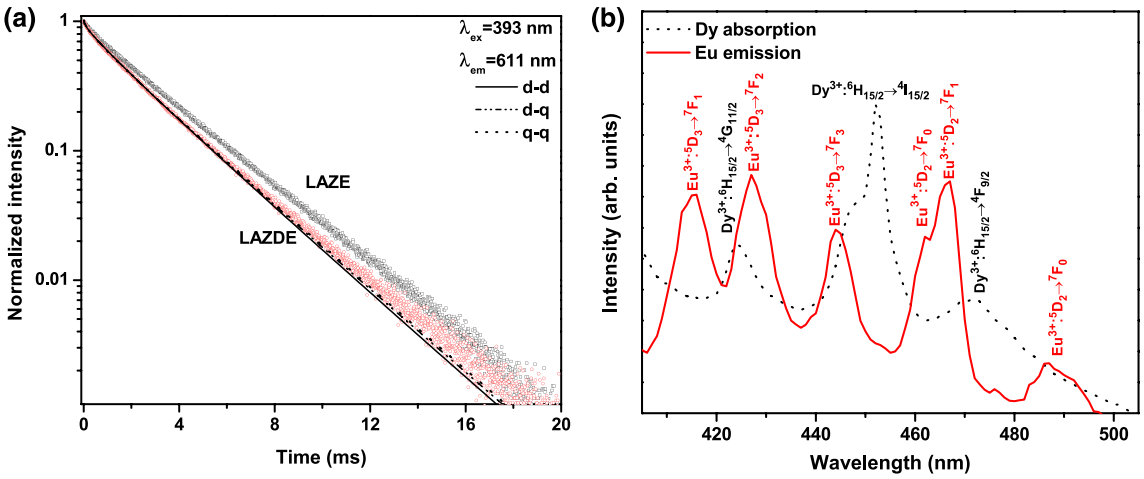

Fig. 6 **a** Eu^{3+} emission at 611 nm for the LAZE and LAZDE glasses. Solid lines represent the best fitting by using Eq. (3), and **b** overlap region of the Eu^{3+} emission and Dy^{3+} absorption

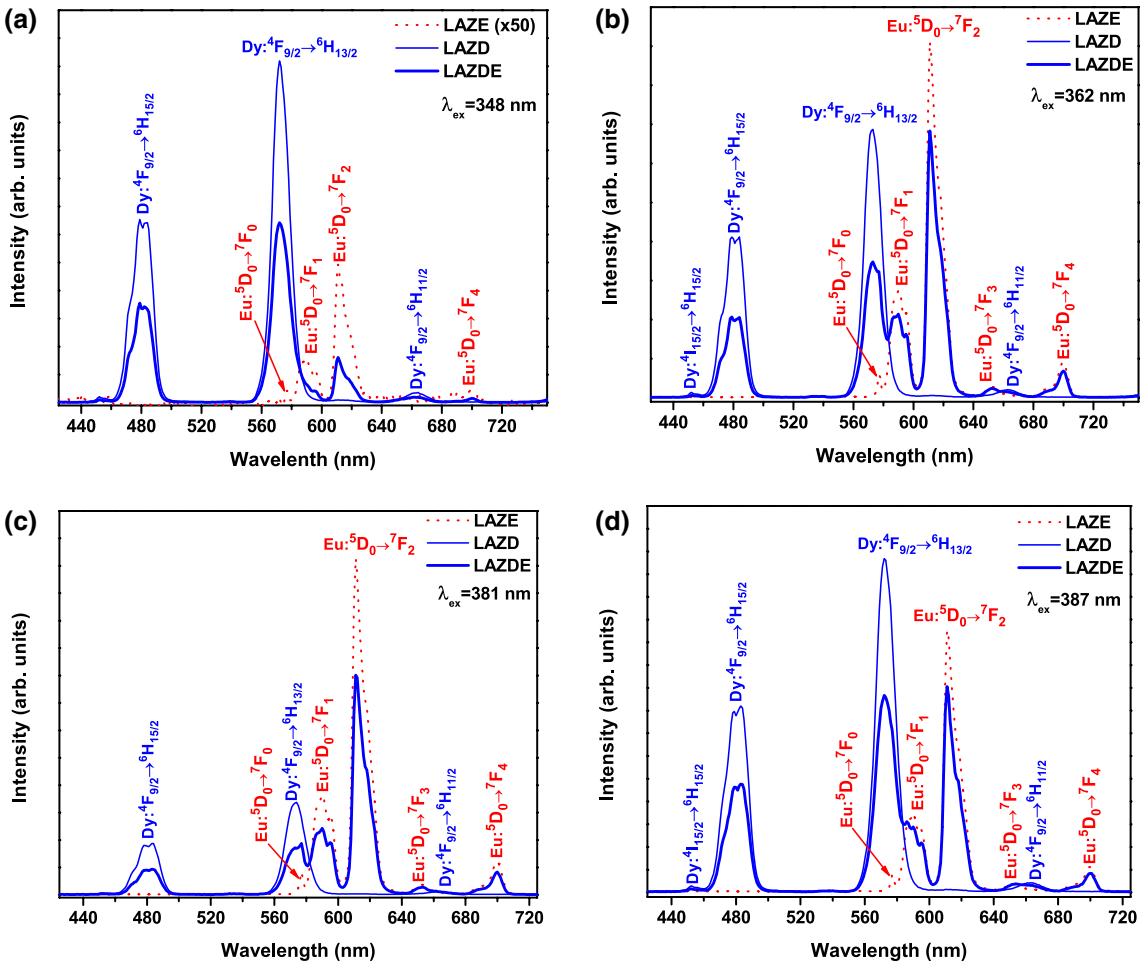

Fig. 7 Emission spectra of the LAZD, LAZE and LAZDE glasses upon excitations at **a** 348, **b** 362, **c** 381 and **d** 387 nm

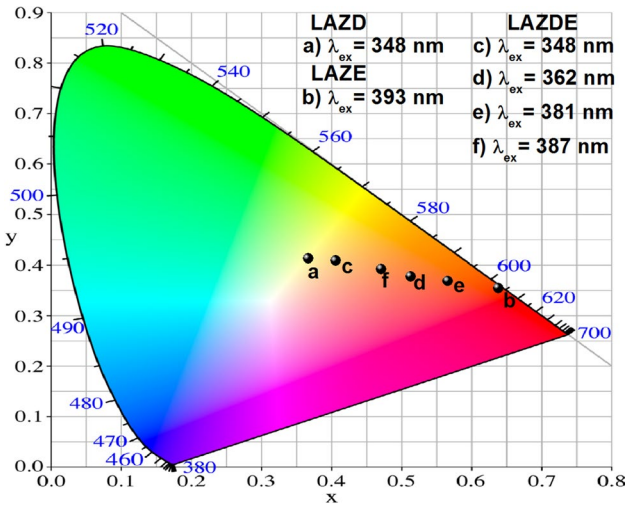

Fig. 8 Chromaticity coordinates in CIE1931 diagram of the global emissions observed in the LAZD, LAZE and LAZDE glasses upon 348, 362, 381 and 387 nm excitations

feature emissions and CIE1931 color chromatic coordinates of the LAZDE glass, upon the excitations above described. The emissions of the LAZD and LAZE singly doped glasses were included for comparison as well. Upon Dy^{3+} excitation [$^6H_{15/2} \rightarrow (^4M_{15/2}, ^6P_{7/2})$] at 348 nm (Fig. 7a), the LAZDE glass exhibits, besides the Dy^{3+}emissions a band located at 611 nm, which is due to the europium $^5D_0 \rightarrow {}^7F_2$ transition. In the LAZDE glass pumped at 348 nm, wherein Eu^{3+} is hardly excited (Figs. 4a, 7a), the Eu^{3+} ($^5D_0 \rightarrow {}^7F_2$) red emission is achieved at expensed of Dy^{3+} $\rightarrow$ Eu^{3+} energy transfer. This fact allows to obtain warm white light emission with $x = 0.406$ and $y = 0.409$ CIE1931 chromaticity coordinates and *CCT* value of 3629 K, evidencing that the Eu^{3+} addition shifts the neutral white emission of the LAZD glass to warm one (Fig. 8). Under dysprosium $^6H_{15/2} \rightarrow {}^4I_{11/2}$ and europium $^7F_0 \rightarrow {}^5D_4$ co-excitations at 362 nm, the dominant Eu^{3+} emission in the LAZDE glass (Fig. 7b) produces reddish-orange tonality with $x = 0.513$ and $y = 0.377$ CIE1931 chromaticity coordinates, *CCT* value of 1839 K and red color purity of 71.7%

Table 1 CIE1931 color chromaticity coordinates, correlated color temperature (*CCT*), dominant wavelength (λ_d), red color purity and emission tonality of the glasses LAZD excited at 348 nm, LAZE excited at 393 nm, and LAZDE excited at 348, 362, 381 and 387 nm

Glass	λ_{exc} (nm)	CIE (*x*, *y*)	*CCT* (K)	λ_d (nm)	Purity (%)	Emission color
LAZE	393	(0.638, 0.354)	2070	604	97.2	Reddish-orange
LAZD	348	(0.367, 0.412)	4547	572	-	Neutral white
LAZDE	348	(0.406, 0.409)	3629	577	50.1	Warm white
LAZDE	362	(0.513, 0.377)	1839	593	71.7	Reddish-orange
LAZDE	381	(0.566, 0.368)	1620	599	82.8	Reddish-orange
LAZDE	387	(0.471, 0.392)	2385	588	63.7	Reddish-orange

(Fig. 8). Upon dysprosium $^6H_{15/2} \rightarrow {}^6P_{3/2,5/2}$ and europium $^7F_0 \rightarrow {}^5L_8$ co-excitations at 381 nm (Fig. 7c), the overall emission of the LAZDE glass is within the reddish-orange region with $x=0.566$ and $y=0.368$, *CCT* value of 1620 K and red color purity of 82.8% (Fig. 8). Upon dysprosium $^6H_{15/2} \rightarrow ({}^4K_{17/2}, {}^4M_{19/2,21/2}, {}^4I_{13/2}, {}^4F_{7/2})$ and europium $^7F_0 \rightarrow {}^5L_8$ excitations at 387 nm (Fig. 7d), the overall emission of the LAZDE glass results in reddish-orange light with red color purity of 63.7% (Fig. 8), according to $x=0.471$ and $y=0.392$ CIE1931 coordinates and *CCT* value of 2385 K. In all cases, it can be observed that the emission intensity of the LAZDE glass is lower than that of the Dy^{3+} and Eu^{3+} singly doped glasses, which is associated with energy transfer between Dy^{3+} and Eu^{3+} ions. Finally, from Fig. 8 and Table 1, it can be appreciated that the overall emission of the Dy^{3+} and Eu^{3+} co-doped glass (LAZDE) can be tuned from warm white to reddish-orange light with red color purity in the 50.1–82.8% range, depending on the excitation wavelength, as consequence of the relative Dy^{3+} and Eu^{3+} emission intensities.

4 Conclusions

A spectroscopic analysis was carried out in Dy^{3+}, Eu^{3+} and Dy^{3+}/Eu^{3+} doped lithium-aluminum-zinc phosphate glasses from absorption, excitation and emission spectra, and decay time measurements. It was observed that the Dy^{3+} and Eu^{3+} doped glasses exhibits the absorption edge below than 350 nm, which fulfils the requirements for W-LEDs applications. Reddish-orange emission tonality was obtained in the Eu^{3+} singly doped glass exciting at 393 nm, whereas neutral white emission was generated in the Dy^{3+} singly doped glass upon 348 nm excitation. The Dy^{3+} and Eu^{3+} co-doping allowed shifting the emission tonality from neutral white to warm white, induced by the Eu^{3+}:$^5D_0 \rightarrow {}^7F_2$ red emission contribution, upon excitation of 348 nm. Under excitations at 362, 381 and 387 nm, the emission tonality is located in the reddish-orange region due to the Eu^{3+} dominant red emission. $Dy^{3+} \rightarrow Eu^{3+}$ non-radiative energy transfer, dominated by an electric quadrupole–quadrupole interaction, allows to obtain warm white emission in the Dy^{3+}/Eu^{3+} co-doped glass. Such process was achieved with efficiency and probability values of 0.08 and 89.51 s^{-1}, respectively. The decay time shortening of the Eu^{3+} emission in the Dy^{3+}/Eu^{3+} co-doped glass revealed that $Eu^{3+} \rightarrow Dy^{3+}$ non-radiative energy transfer, mediated by an electric quadrupole–quadrupole interaction, occurs with an efficiency and probability of 0.08 and 30.00 s^{-1}, respectively.

Acknowledgements A.N. Meza-Rocha and R. Lozada-Morales thank Cátedras CONACyT (Grant No. 2801). This work was supported by the CONACYT-CNR bilateral agreement under Project Contract 173855. Authors appreciate the technical support from Laboratorio Central-IFUAP.

References

1. M.C.S. Reddy, B.A. Rao, M.G. Brik, A.P. Reddy, P.R. Rao, C.K. Jayasankar,·N. Veeraiah, Emission characteristics of Dy^{3+} ions in lead antimony borate glasses. Appl. Phys. B. **108**, 455 (2012)
2. A. Lira, A. Speghini, E. Camarillo, M. Bettinelli, U. Caldiño, Spectroscopic evaluation of $Zn(PO_3)_2$:Dy^{3+} glass as an active medium for solid state yellow laser. Opt. Mater. **38**, 188 (2014)
3. J.L. Cai, R.Y. Li, C.J. Zhao, S.L. Tie, X. Wan, J.Y. Shen, White light emission and energy transfer in Dy^{3+}/Eu^{3+} co-doped aluminoborate glass. Opt. Mater. **34**, 1112 (2012)
4. V.R. Bandi, B.K. Grandhe, H.-J. Woo, K. Jang, D.-S. Shin, S.-S. Yi, J.-H. Jeong, Luminescence and energy transfer of Eu^{3+} or/and Dy^{3+} co-doped in Sr_3AlO_4F phosphors with NUV excitation for WLEDs. J. Alloys Compd. **538**, 85 (2012)
5. E. Pavitra, G. Seeta Rama Raju, J.S. Yu, White light emission from Eu^{3+} co-activated $Ca_2Gd_8Si_6O_{26}$:Dy^{3+} nanophosphors by solvothermalsynthesis. Ceram. Int. 39 (2013) 6319.
6. S. Das, A.A. Reddy, S.S. Babu, G.V. Prakash, Controllable white light emission from Dy^{3+}–Eu^{3+} co-doped $KCaBO_3$ phosphor. J. Mater. Sci. **46**, 7770 (2011)
7. J. Massera, K. Bourhis, L. Petit, M. Couzi, L. Hupa, M. Hupa, J.J. Videau, T. Cardinal, Effect of the glass composition on the chemical durability of zinc-phosphate-based glasses in aqueous solutions. J. Phys. Chem. Solids **74**, 121 (2013)
8. R.K. Brow Review: the structure of simple phosphate glasses, J. Non-Cryst. Solids **263–264**, 1 (2000)
9. H. Zhong, G. Chen, L. Yao, J. Wang, Y. Yang, R. Zhang, The white light emission properties of $Tm^{3+}/Tb^{3+}/Sm^{3+}$ triply doped SrO–ZnO–P_2O_5 glass. J. Non-Cryst. Solids **427**, 10 (2015)
10. S. Li, S. Huang, F. Wu, Y. Yue, Structure and properties of zinc aluminophosphate glasses and those doped with zirconium dioxide. J. Non-Cryst. Solids **419**, 45 (2015)
11. H.-J. Zhong, G.-H. Chen, S.-C. Cui, J.-S. Chen, Y. Yang, C.-R. Zhou, C.-L. Yuan, Luminescence and energy transfer of Tm/Tb/

Mn tri-doped phosphate glass for white light-emitting diodes. J. Mater. Sci. **26**, 8130 (2015)
12. C.S. McCamy, Correlated color temperature as an explicit function of chromaticity coordinates. Color. Res. Appl. **17**, 142 (1992)
13. A.N. Meza-Rocha, I. Camarillo, R. Lozada-Morales, U. Caldiño, Reddish-orange and neutral/warm white light emitting phosphors: Eu^{3+}, Dy^{3+} and Dy^{3+}/Eu^{3+} in potassium-zinc phosphate glasses. J. Lumin. **183**, 341 (2017)
14. C.R. Kesavulu, C.K. Jayasankar, White light emission in Dy^{3+}-doped lead fluorophosphate glasses. Mater. Chem. Phys. **130**, 1078 (2011)
15. A.N. Meza-Rocha, A. Speghini, M. Bettinelli, U. Caldiño, White light generation through $Zn(PO_3)_2$ glass activated with Eu^{3+} and Dy^{3+}. J. Lumin. **176**, 235 (2016)
16. U. Caldiño, A. Speghini, M. Bettinelli, Optical spectroscopy of zinc metaphosphate glasses activated by Ce^{3+} and Tb^{3+} ions. J. Phys. **18**, 3499 (2006)
17. D.A. Rodríguez-Carvajal, A.N. Meza-Rocha, U. Caldiño, R. Lozada-Morales, E. Alvarez, M.E. Zayas, Reddish-orange, neutral and warm white emissions in Eu^{3+}, Dy^{3+} and Dy^{3+}/Eu^{3} doped $CdO\text{-}GeO_2\text{-}TeO_2$ glasses. Solid State Sci. **61**, 70 (2016)
18. P. Villanueva-Delgado, K.W. Kramer, R. Valiente, M. de Jong, A. Meijerink, Modeling blue to UV upconversion in $\beta\text{-}NaYF_4:Tm^{3+}$. Phys. Chem. Chem. Phys. **18**, 27396 (2016)
19. U. Caldiño, Energy transfer in CaF_2 doped with Ce^{3+}, Eu^{2+} and Mn^{2+} ions, J. Phys. **15**, 7127 (2003)
20. T. Nishida, T. Ban, N. Kobayashi, 340–350 nm GaN-free UV-LEDs. Phys. Status Solidi A **200**, 106 (2003)
21. S. Guha, N.A. Bojarczuk, Ultraviolet and violet GaN light emitting diodes on silicon. Appl. Phys. Lett. **72**, 415 (1998)
22. Q. Zeng, P. He, H.B. Liang, M. Gong, Q. Su, Luminescence of Eu^{3+}-activated tetra-molybdate red phosphors and their application in near-UV InGaN-based LEDs. Mater. Chem. Phys. **118**, 76 (2009)